Structural Ordering and Ferromagnetism in $La_4Mn_4O_{11}$

M. L. Ruiz-González,[†] R. Cortés-Gil,[†,‡] J. M. Alonso,[‡,§] A. Hernando,[‡,∥] M. Vallet-Regí,[‡,⊥] and J. M. González-Calbet*[,†,‡]

Departamento de Química Inorgánica, Facultad de Químicas, Departamento de Física de Materiales, Facultad de Físicas, and Departamento de Química Inorgánica y Bioinorgánica, Facultad de Farmacia, Universidad Complutense, 28040 Madrid, Spain, Instituto de Magnetismo Aplicado, UCM-CSIC-ADIF, Las Rozas, P.O. Box 155, 28230 Madrid, Spain, and Instituto de Ciencia de Materiales, CSIC, Sor Juana Inés de la Cruz s/n, 28049 Madrid, Spain

Received April 20, 2006. Revised Manuscript Received July 24, 2006

Electron diffraction and high-resolution electron microscopy of $LaMnO_{3-\delta}$ ($0 \leq \delta \leq 0.25$), obtained by topotactic reduction of $LaMnO_3$, shows that an ordered pathway of anionic vacancies is only obtained for $\delta = 0.25$. $La_4Mn_4O_{11}$ is an eightfold superlattice of the perovskite-type structure due to the ordered intergrowth of three octahedral layers and one tetrahedral layer along the *b* axis, according to the sequence ...OOOTOOOT′... The reduced sample exhibits ferromagnetic behavior with $T_c \approx 50$ K. The staircase effect, observed at low temperature, is discussed in terms of the magnetic ordering adopted in the octahedral layers.

Introduction

Moved by the need to improve device applications based on the colossal magnetoresistance effect,[1] considerable effort has been devoted to the study of the physical properties of manganese perovskite (ABO_3) related oxides. The ability of Mn to adopt several oxidation states plays an important role in the different and complex magnetic behaviors they adopt. In most of the previous work in mixed-valence manganese perovskites, hole doping is induced by the substitution of a rare-earth ion by an alkaline-earth divalent ion in $LaMnO_3$, every substituted divalent cation creating a hole (h^+) in the e_g Mn levels. These materials show two transitions related to the presence of Mn^{IV} and Mn^{III} that interact through a shared oxygen[2]: (i) from a low-temperature ferromagnetic (FM) to a high-temperature paramagnetic state and (ii) from metal to insulator, in the close neighborhood of the Curie temperature, T_c.

Mn^{IV} holes can also be generated by oxidation of the initial $LaMnO_3$, an orthorhombic distorted perovskite due to the Jahn−Teller effect.[3] The stoichiometric compound, an antiferromagnetic (AFM) insulator material,[4] can be oxidized leading to $La_{1-t}Mn_{1-t}O_3$[5−8] (so-called $LaMnO_{3+\delta}$) which shows FM and metallic behavior.[9−12] The oxygen content decrease would lead to Mn^{II} formation being the structural and magnetic properties affected. Although initially thought that oxygen deficiency could not be accommodated in $LaMnO_3$ because the Mn^{II} ionic radius[13] is too large to be fitted in the B perovskite sublattice, Kamata et al.[14] suggested that some $LaMnO_{3-\delta}$ phase is stabilized after decomposition of the stoichiometric material at low oxygen partial pressures at 1473 K. Moreover, Hansteen et al.[15] have prepared $LaMnO_{3-\delta}$ ($0.08 < \delta < 0.25$) samples by zircothermal reduction of $LaMnO_3$. In this way, an A-type antiferromagnetically ordered[4] orthorhombic *Pnma* $LaMnO_{2.8}$ phase is obtained, with anionic vacancies randomly distributed, the diffraction profile showing some weak and broad reflections due to minor inclusions of three impurity phases, La_2O_3, MnO, and $LaMnO_{2.92}$, corresponding to a weight fraction of 24%.

The introduction of anionic vacancies must necessarily affect both structural and magnetic properties. Nonstoichiometry studies at the oxygen sublattice have been performed in the La−Ca−Mn−O system leading to the stabilization

* To whom correspondence should be addressed. E-mail: jgcalbet@quim.ucm.es. Fax: 34 91 394 43 52.
† Departamento de Química Inorgánica, Facultad de Químicas, Universidad Complutense.
‡ UCM-CSIC-ADIF.
§ CSIC.
∥ Departamento de Física de Materiales, Facultad de Físicas, Universidad Complutense.
⊥ Departamento de Química Inorgánica y Bioinorgánica, Facultad de Farmacia, Universidad Complutense.

(1) von Helmholt, R. M; Wecker, J.; Holzapfel, B.; Schultz, L.; Samwer, K. *Phys. Rev. Lett.* **1993**, *71*, 2331.
(2) Zener, C. *Phys. Rev.* **1951**, *81*, 440; *82*, 403.
(3) Elemans, J. B. A. A.; Van Laar, B.; Van der Veen, K. R.; LoopStra, B. O. *J. Solid State Chem.* **1971**, *3*, 238.
(4) Wollan, E. O.; Koehler, W. C. *Phys. Rev.* **1955**, *100*, 545.
(5) Van Roosmalen, J. A. M.; Cordfunke, E. H. P.; Helmholdt, R. B.; Zandbergen, H. W. *J. Solid State Chem.* **1994**, *110*, 100.
(6) Van Roosmalen, J. A. M.; Cordfunke, E. H. P. *J. Solid State Chem.* **1994**, *110*, 106.
(7) Van Roosmalen, J. A. M.; Cordfunke, E. H. P. *J. Solid State Chem.* **1994**, *110*, 109.
(8) Van Roosmalen, J. A. M.; Cordfunke, E. H. P. *Solid State Chem.* **1994**, *110*, 113.
(9) Verelst, M.; Rangavittal, N.; Rao, C. N. R.; Rousset, A. *J. Solid State Chem.* **1993**, *104*, 74.
(10) Mahendiran, R.; Tiwary, S. K.; Raychaudhuri, A. K.; Ramakrishnan, T. V.; Mahesh, R.; Rangavittal, N.; Rao, C. N. R. *Phys. Rev. B* **1996**, *53*, 3348.
(11) Huang, A.; Santoro, J. W.; Lynn, R. W.; Erwin, J. A.; Borchers, J. L.; Greene, R. L. *Phys. Rev. B* **1997**, *55*, 14987.
(12) Prado, F.; Sánchez, R. D.; Caneiro, A; Causa, M. T.; Tovar, M. *J. Solid State Chem.* **1999**, *146*, 418.
(13) Shannon, R. D. *Acta Crystallogr., Sect. A* **1976**, *32*, 751.
(14) Kamata, K.; Nakajima, T.; Hayashi, T.; Nakamura, T. *Mater. Res. Bull.* **1978**, *13*, 49.
(15) Hansteen, O. H.; Bréard, Y.; Fjellvag, H.; Hauback, B. C. *Solid State Sci.* **2004**, *6*, 279.

10.1021/cm0609193 CCC: $33.50
Published on Web 11/01/2006

of the $La_{0.5}Ca_{0.5}MnO_{2.5}$ phase that shows the brownmillerite structure.[16] This type can be described from the ordered intergrowth of tetrahedral and octahedral layers according to the stacking sequence ...OTOT′... (O = octahedron, T = tetrahedron). The second tetrahedral layer (T′) is tilted with respect to the first one (T) leading to a $b \cong 4a_c$ parameter (subscript c stands for the cubic perovskite sublattice). In the Ca free system, the stabilization of the $La_4Mn_4O_{11}$ ($LaMnO_{2.75}$) composition has been proposed,[17] where anionic vacancies lie on the $[110]_c$ direction. The above composition is the one required for the stabilization of the $n = 4$ term of the homologous series $A_nB_nO_{3n-1}$,[18,19] reported for the $Ca_4Ti_2Fe_2O_{11}$ compound, which can be described as an eightfold perovskite superlattice along the *b* axis due to the ordered intergrowth of octahedral and tetrahedral layers according to the sequence ...OOOTOOOT′... The meaning of T and T′ is the same as already described in the brownmillerite type structure leading to an eightfold superlattice instead of a fourfold one.

On the basis of this information, we have undertaken a study of the influence of the oxygen deficiency in the $LaMnO_{3-\delta}$ system, prepared by topotactic reduction of $LaMnO_3$. Preliminary studies[20] have shown that compositional variations in the range ($0.03 \leq \delta \leq 0.12$) lead to a phase mixture. This situation is in agreement with the reported difficulty to stabilize intermediate phases,[21,22] built up of ordered sequences of octahedral and tetrahedral layers, between perovskite and brownmillerite when the oxygen deficiency is close to $\delta = 0$. Actually, based on theoretical calculations, Komornicki et al.[23] hypothesized that the vacancy ordering varies continuously as a function of the oxygen deficiency. For values of δ close to 0.15, anionic deficiency was thought to be ordered along rows of different length in a statistical fashion, these developing into vacancy rows of infinite length for δ close to 0.20. When δ approaches to 0.25, vacancy rows order into planes giving rise to local disordered intergrowths, which become ordered by increasing either the annealing times[18] or the oxygen deficiency.[17,21,22,24] In this paper, we study the ordered pathway of anionic vacancies in $LaMnO_{2.75}$, that is, $La_4Mn_4O_{11}$, by means of X-ray and selected area electron diffraction (SAED) and high-resolution electron microscopy (HREM). The magnetic behavior is studied by means of magnetization measurements as a function of the temperature and hysteresis loops. Relationships between structural and magnetic behavior is discussed.

Experimental Section

The starting material, $LaMnO_{3.03}$, was synthesized by the ceramic method. Stoichiometric amounts of La_2O_3 and MnO_2 were homogenized and milled in one agate mill and heated at 1400 °C for 100 h, with several intermediate grindings. After quenching in liquid nitrogen, a single phase is obtained. Cationic composition, as determined by X-ray energy dispersive spectroscopy (EDS), leads to a La/Mn = 1:1 ratio.

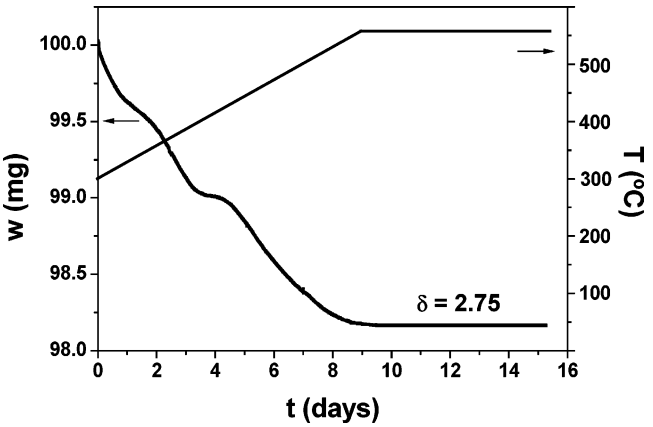

Figure 1. Thermogravimetric curve corresponding to the $LaMnO_{3.03} \rightarrow LaMnO_{2.75}$ reduction process.

Oxygen content was inferred by thermogravimetric analysis using a Cahn D-200 electrobalance equipped with a furnace and a two-channel register, allowing simultaneous recording of the weight loss and the reaction temperature. The sample was heated in a H_2 (200 mbar) and He (300 mbar) atmosphere until 800 °C at a 6 °C/min ratio. The analysis of the reduction products (La_2O_3 and MnO) and the weight loss together with the cationic stoichiometry data indicates the stabilization of a sample with the general formula $LaMnO_{3.03}$, involving Mn^{3+} (94%) and Mn^{4+} (6%). This sample (~100 mg) was reduced in the electrobalance in a H_2 (200 mbar) and He (300 mbar) atmosphere at the heating rate of 6 °C/min until 300 °C (temperature at which reduction starts) and, once reached, at 0.02 °C/min until 560 °C, leading to the thermogravimetric reduction shown in Figure 1. A *plateau* at 560 °C, corresponding to oxygen content of 2.75 per formula unit, is observed. The sample was annealed during some days at the target temperature (560 °C), under He atmosphere (500 mbar). The oxygen content establishes the Mn^{3+}/Mn^{2+} ratio which, together with the EDS analysis, leads to the $LaMn_{0.5}^{3+}Mn_{0.5}^{2+}O_{2.75}$, that is, $La_4Mn_2^{3+}Mn_2^{2+}O_{11}$ composition.

X-ray diffraction (XRD) patterns were obtained in a Philips X'Pert (Cu Kα radiation) diffractometer. Microstructural characterization was carried out on both JEOL 2000 FX and JEM-3000F electron microscopes equipped with microanalysis systems (Oxford Instruments). Magnetic measurements were performed on a Quatum Desing SQUID magnetometer (MPMS).

Results and Discussion

The XRD pattern of the parent material, $LaMnO_{3.03}$, can be indexed, as expected,[3] on the basis of an orthorhombic unit cell, $a_c\sqrt{2}$, $2a_c$, $a_c\sqrt{2}$ ($a = 0.535(2)$ nm, $b = 0.707(2)$ nm, $c = 0.567(2)$ nm), while a clear change is observed for the reduced sample (Figure 2). In the case of $La_4Mn_4O_{11}$, superstructure reflections are evident (see inset), probably due to ordering of anionic vacancies. Actually, the XRD

(16) González-Calbet, J. M.; Herrero, E.; Rangavittal, N.; Alonso, J. M.; Martínez, J. L.; Vallet-Regí, M. *J. Solid State Chem.* **1999**, *148*, 158.
(17) Abbattista, F.; Borlera, M. L. *Ceram. Int.* **1981**, *7*, 137.
(18) González-Calbet, J. M.; Vallet-Regí, M. *J. Solid State Chem.* **1987**, *68*, 266.
(19) Hovmoller, S.; Zou, X.; Wang, D. N.; González-Calbet, J. M.; Vallet-Regí, M. *J. Solid State Chem.* **1988**, *77*, 316.
(20) Cortés-Gil, R.; Arroyo, A.; Ruiz-González, L.; Alonso, J. M.; Hernando, A.; González-Calbet, J. M.; Vallet-Regí, M. *J. Phys. Chem. Solids* **2005**, *67*, 579.
(21) Alario-Franco, M. A.; González-Calbet, J. M.; Vallet-Regí, M. *J. Solid State Chem.* **1986**, *65*, 383.
(22) González-Calbet, J. M.; Alonso, J. M.; Vallet-Regí, M. *J. Solid State Chem.* **1987**, *71*, 331.
(23) Komornicki, S.; Grenier, J. C.; Pouchard, M.; Hagenmuller, P. *Nuovo J. Chim.* **1981**, *5*, 161.
(24) Grenier, J. C.; Pouchard, M.; Hagenmuller, P. *C. R. Acad. Sci.* **1977**, *285* (c), 527.

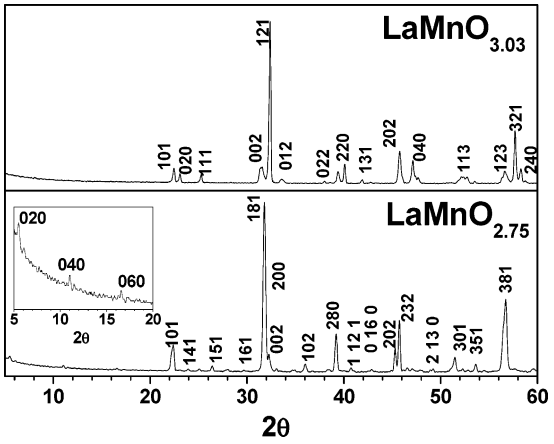

Figure 2. Powder XRD patterns of $LaMnO_{3.03}$ and $La_4Mn_4O_{11}$. Notice that (*hkl*) indices are only shown for the most intense peaks.

pattern (Figure 2) can be indexed on the basis of an eightfold orthorhombic perovskite superstructure,[17] isostructural to $Ca_4Fe_2Ti_2O_{11}$,[18] with parameters $a = 0.562(1)$ nm, $b = 3.200(1)$ nm, and $c = 0.559(1)$ nm (space group *Pnma*), characteristic of the $n = 4$ term of the $A_nB_nO_{3n-1}$ homologous series. No impurity phases have been detected.

At this point, it is worth mentioning that diffraction maxima are slightly broad. This is a quite frequent fact in samples obtained at low target temperatures. Actually, the reduction process $LaMnO_3 \rightarrow LaMnO_{2.75}$ takes place at 560 °C, and further temperature increase leads to decomposition of the reduced material. The XRD pattern can be indexed on the basis of an eightfold perovskite cell,[17−18] but its quality, due to the inherent characteristics of the synthesis procedure, is not high enough for Rietveld refinement. Moreover, the broadening of the diffraction peaks suggests the presence of small structural domains in the material as previously reported for isostructural $Ca_4Fe_2Ti_2O_{11}$.[25] It is in fact well-known that oxygen deficient perovskite related phases usually exhibit local order phenomena that in some cases cannot be detected by XRD techniques, a microstructural study being required for a better understanding. In this sense, a microstructural characterization, by means of SAED and HREM, has been performed for $La_4Mn_4O_{11}$.

The SAED study is in agreement with the $a_c\sqrt{2} \times 8a_c \times a_c\sqrt{2}$ unit cell, although some additional features have been detected. Actually, the eightfold superlattice along the b^* direction is clearly observed in the pattern along $[10\bar{1}]$ (Figure 3a). Notice, however, that equivalent superlattice reflections, pointed out by vertical bars at the pattern, appear along the perpendicular reciprocal direction, suggesting a similar superstructure or the presence of perpendicular domains, as reported in many related perovskite systems.[26,27] This option seems to be more plausible because a set of spots disappears when the pattern is obtained in a different, but very close, area of the same crystal (Figure 3b). Moreover, both patterns (Figure 3a,b, respectively) show additional spots, arrowed, doubling the [181] direction, that have not yet been explained. It can be, again, understood on the basis of a third perpendicular domain, that is, the presence of [010] areas. Figure 3c shows the characteristic SAED pattern along the [010] zone axis. Notice that the forbidden reflection (100), usually present as a consequence of multiple scattering processes, justifies the additional spots appearing in Figure 3a,b. It is then clear that the coexistence of three perpendicular domains gives rise to the pattern depicted in Figure 3a, as schematically represented at the calculated patterns in Figure 3f−h. These calculated patterns as well as the corresponding image calculations have been performed on the basis of previous information of the deduced model for the $n = 4$ term $Ca_4Fe_2Ti_2O_{11}$.[18,19] Atomic coordinates are summarized in Table 1.

Starting from the $[10\bar{1}]$ projection and tilting 45° around the *b* axis, the pattern shown in Figure 3d is obtained. It can be indexed on the basis of the [100] zone axis, again, the the presence of additional spots (arrowed) doubling, in this case, the [082]* direction being remarkable. These extra reflections can be explained keeping in mind the coexistence of the [010] domain and considering, also, its 45° tilt. This rotation leads to the $[41\bar{4}]$ projection, as represented in the calculated pattern (Figure 3i). Notice that the overlapping of the calculated SAED patterns along $[41\bar{4}]$ and [100], Figure 3i,j, respectively, does not justify the additional spot arrowed on the experimental one (Figure 3d) that must appear, again, because of the frequently effect of multiple scattering. To confirm this domain description, a HREM study has been carried out.

Figure 4a is an image along $[10\bar{1}]$ corresponding to the pattern displayed in Figure 3b. Areas exhibiting different periodicities are evident. The superlattice along *b*, showing spacing of $d_{020} = 1.62$ nm, is clear at the zone marked as A, whereas distances characteristic of $d_{200} = 0.27$ nm are apparent in the zones labeled as B. Such features are confirmed by the corresponding FT (Fourier transform), performed in each area (Figure 4b,c). These two FTs clearly confirm the experimental SAED pattern as a consequence of the intergrowth of two perpendicular domains along $[10\bar{1}]$ (Figure 4b) and [010] (Figure 4c).

For a better understanding, an image calculation was performed taking into account the atomic positions derived from the model ...OOOTOOOT′... and parameters obtained by XRD. Figure 5a is an enlarged image of the A domain, where the calculated image (Figure 5b) at defocus $\Delta f = 0$ nm and thickness $\Delta t = 6$ nm has been inserted. A good agreement between both experimental and calculated images can be observed. A model along the projection $[10\bar{1}]$, superimposed to a magnified detail of the image, is depicted in Figure 5c.

Figure 6a is a HREM image along the [100] zone axis, that is, corresponding to the SAED pattern depicted in Figure 3d. Areas showing different periodicities, marked as C, D, and E, are, again, observed. C and D areas show distances of 3.24 and 1.62 nm, respectively, along *b*, being in agreement with the ones detected on the model ...OOOTOOOT′... along the [100] and [001] zone axis. This can be better understood on the basis of the schematic projections shown

(25) González-Calbet, J. M.; Vallet-Regí, M. *Inst. Phys. Conf. Ser.* **1988**, *2* (93), 277 (Chapter 7).
(26) Vallet-Regí, M.; González-Calbet, J. M.; Alario-Franco, M. A.; Grenier, J. C.; Hagenmuller, P. *J. Solid State Chem.* **1984**, *55*, 251.
(27) Vegas, A.; Vallet-Regí, M.; González-Calbet, J. M.; Alario-Franco, M. A. *Acta Crystallogr.* **1986**, *42*, 167.

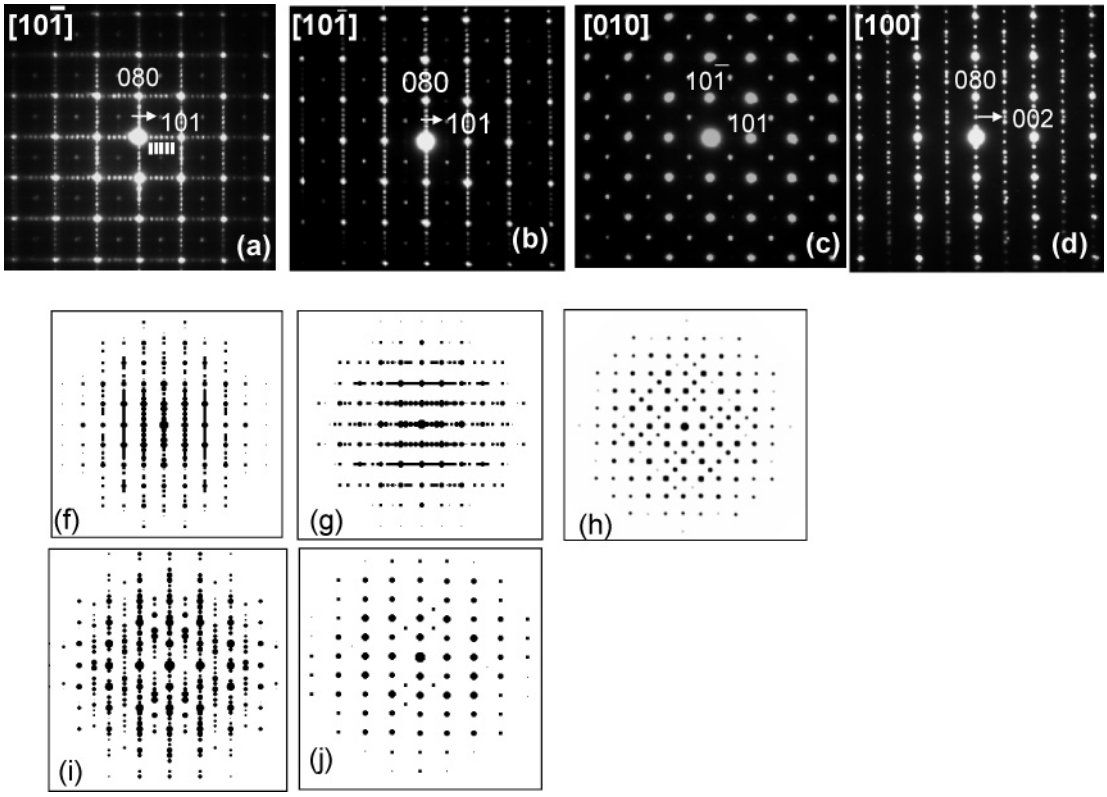

Figure 3. SAED diffraction patterns corresponding to $La_4Mn_4O_{11}$ along (a) [10$\bar{1}$] (showing three domains), (b) [10$\bar{1}$] (showing two domains), and (c) [010] and (d) [100] and calculated patterns (f−j).

Table 1. Atomic Positions Corresponding to $La_4Mn_5O_{11}$ Used for Diffraction and Images Calculations

atom	*x*/*a*	*y*/*b*	*z*/*c*	occ.
Mn(1)	0.0000	0.0000	0.0000	1
Mn(2)	−0.0500	0.2500	0.0000	1
Mn(3)	0.0000	0.1250	0.0000	1
La	0.5000	0.0625	0.0000	1
La	0.5000	0.1875	0.0000	1
O(1)	0.2500	0.0000	0.2500	1
O(2)	0.0000	0.0625	0.0000	1
O(3)	0.2500	0.1250	0.2500	1
O(4)	0.25	0.125	0.75	1
O(5)	0.6000	0.2500	0.1000	1
O(6)	0.0000	0.1875	0.0000	1

in Figure 6b. The calculated image along [001] is displayed on Figure 7. A good agreement between experimental and calculated images is observed. The third domain, marked as E in Figure 6, is related to the B areas observed in Figure 4 as a consequence of the 45° tilting, previously described. The rotation leads to the [41$\bar{4}$] projection as confirmed by the corresponding FT (Figure 6c).

Magnetization measurements as a function of the temperature were performed under different applied fields in zero field cooling (ZFC) and field cooling (FC) conditions, as shown in Figure 8. As can be observed, the material shows two different behaviors as a function of applied magnetic field. Down to 0.1 T, the magnetization, at the lowest temperatures, in ZFC conditions shows a near zero magnetization value whereas in FC conditions it shows a value that increases as the applied magnetic field increases. This magnetic evolution can be related to a ferrimagnetic, that is, noncompensated, AFM behavior. However, at higher applied magnetic fields, the evolution of magnetization

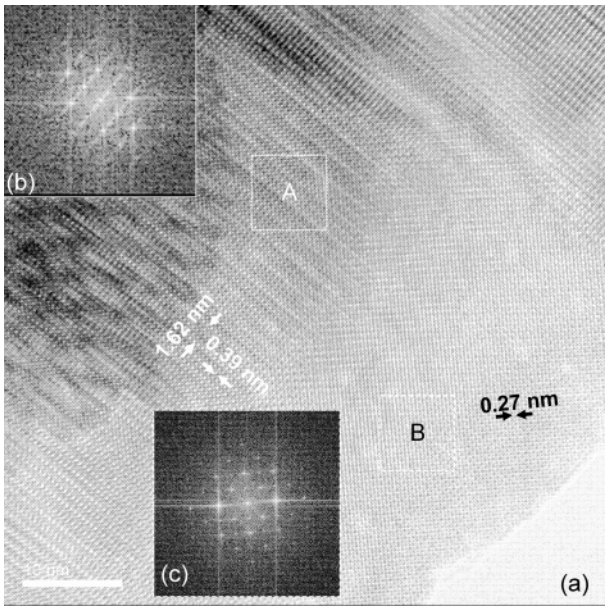

Figure 4. (a) HREM image along [10$\bar{1}$]. Areas of different periodicities, A and B, are observed. (b) FT corresponding to area A and (c) FT corresponding to B area.

suggests a FM behavior, with $T_c \sim 50$ K, obtained from the derivate of the FC curves. The inverse of the magnetization is also represented in Figure 8, where a linear fit of the evolution leading to $\theta_w > 0$ values can be clearly observed in the range $150 < T < 300$ K. This fact indicates the existence of FM interactions at the paramagnetic region. For a better understanding of this behavior, magnetization measurements as a function of the applied field at different temperatures have been performed.

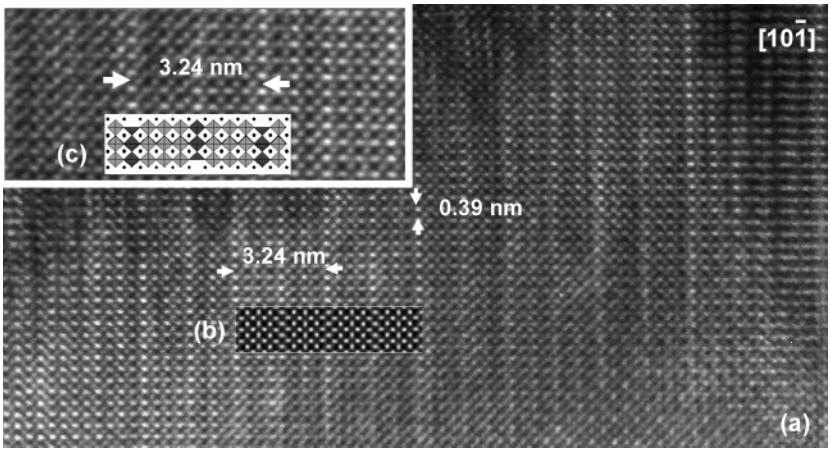

Figure 5. (a) Enlarged image of the A domain. (b) Calculated image and (c) polyhedra model.

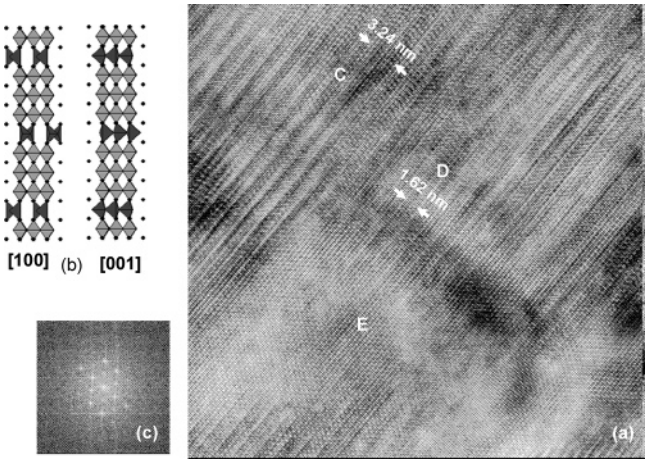

Figure 6. (a) HREM image where areas corresponding to three orientations, C, D, and E, [100], [001], and [41$\bar{4}$], respectively, are evident. (b) Polyhedra model along [100] and [001]. (c) FT of area E.

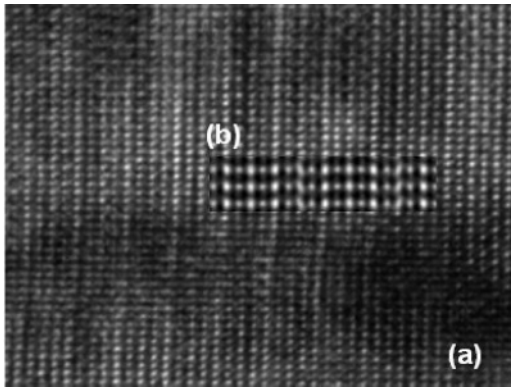

Figure 7. (a) Enlarged image of the D domain. (b) Corresponding calculated image.

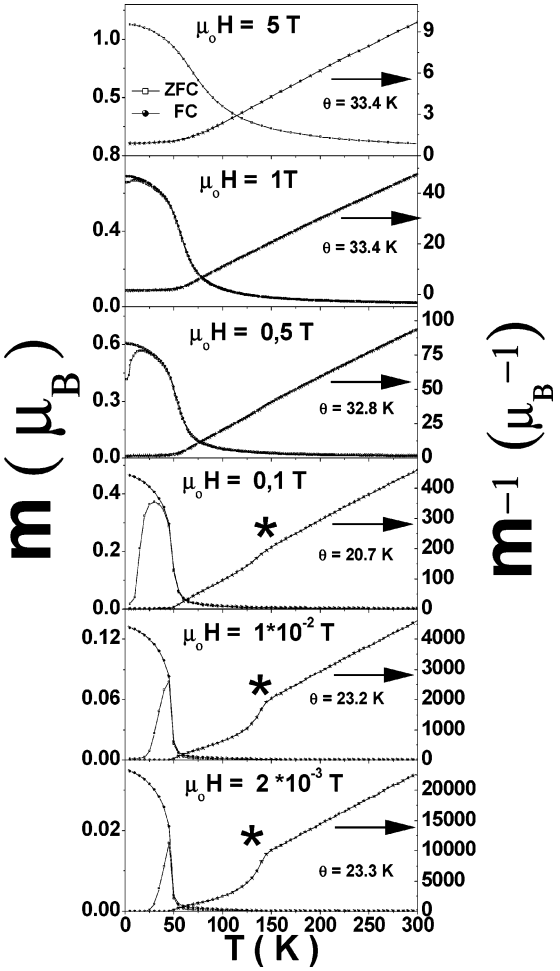

Figure 8. ZFC and FC magnetization measurements and the inverse of the FC magnetization of $La_4Mn_4O_{11}$ as a function of the temperature at different applied fields.

Figure 9 clearly shows hysteresis loops between 2 and 40 K which correspond to a FM behavior with a maximum value of magnetization of 1.14 μ_B at 5 T and 2 K. It is worth emphasizing that the loop is not saturated under these conditions. The extrapolation of the hysteresis loop leads to a saturation magnetization value of 1.4 μ_B at $\mu_0 H = 20$ T. This value is very small taking into account the presence of Mn^{2+} (5.8 μ_B) and Mn^{3+} (4.9 μ_B). This apparently anomalous behavior will be explained in the following.

At higher temperature ($T \geq 80$ K), the variation of the magnetization versus field shows a clear paramagnetic behavior. It is worth stressing that coercive field values gathered in Table 2 reveal that in the range 40−2 K these field values increase more than 2 orders of magnitude. A more careful inspection of the hysteresis loops shows that at 2 and 5 K, the magnetization undergoes a staircase effect (see inset at Figure 9) which disappears at higher temperatures. The initial magnetization curve at 5 K exhibits a remarkable stepwise variation at around 0.2 T, labeled stage

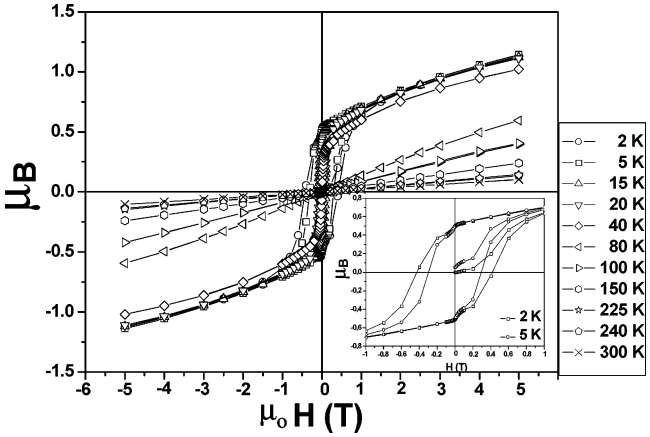

Figure 9. Magnetization curves of $La_4Mn_4O_{11}$ as a function of the magnetic field. Hysteresis loops at 2 and 5 K are shown at the inset.

Table 2. Coercive Field and Remmant Magnetization (mr) Values at Different Temperatures for $La_4Mn_4O_{11}$

T (K)	coercive field (T)	m_r (μ_B)
2	4.2×10^{-1}	0.67
5	3.0×10^{-1}	0.67
15	1.0×10^{-1}	0.65
20	5.7×10^{-2}	0.64
40	2.5×10^{-3}	0.55

1 in Figure 10a. Once this applied field is reached, magnetization increases (stage 2) up to a maximum value of 1.14 μ_B at 5 T, as previously shown in Figure 9. Magnetization decreases from 5 to 0 T, and a staircase effect appears, down to 0.2 T, when the reversed field magnetization is applied (stage 3) and then the hysteresis loop develops a normal behavior (stage 4) until zero applied field, where the material shows the same staircase effect (stage 5). Finally, to close the loop, the curve in stage 6 is symmetrical to the one observed in stage 4. The staircase appearance in the $0.2 < \mu_0 H_c < 0.3$ T (H_c, critical field) range is clearly observed in Figure 10b. Besides, the staircase effect gives rise to an increase of the coercive field of more than two orders of magnitude. A somewhat similar effect has been observed in other perovskite related oxides.[28] In particular, in $Ba_5Co_5O_{14}$, due to the nuclear structure, it has been proposed that this effect seems to be related to a very stable domain structure obtained after cooling from room temperature. The stability of this stair effect seems to be similar to that observed in FM materials in which the magnetic domains are related to the crystallographic ones. In the case of manganites, showing CE-type AFM structure,[29−31] the phenomenon has been mainly observed in Mn-site substituted compounds.[29,30] In this sense, Hardy et al.[31] suggest that the staircase-like stage observed in Ga doped $Pr_{0.5}Ca_{0.5}MnO_3$ can be interpreted on the basis of structural distortions associated to the collapse of the orbital ordering. However, they also show that the phenomenon also appears in $Pr_{0.63}Ca_{0.37}MnO_3$ where foreign

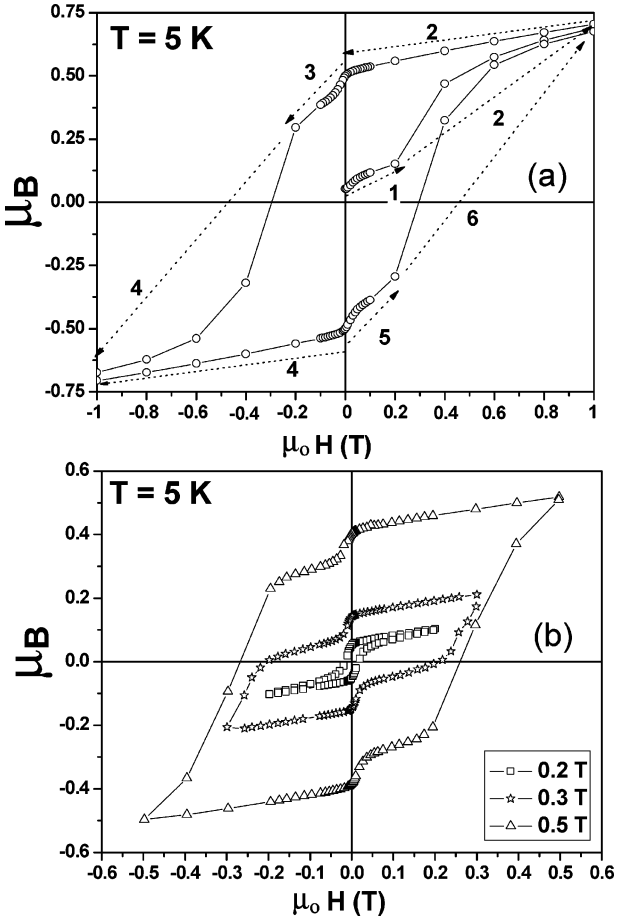

Figure 10. (a) Enlargement of $La_4Mn_4O_{11}$ hysteresis loop at 5 K, showing six remarkable stages. (b) Hysteresis loops at 5 K at different maximum applied magnetic fields.

cations at the Mn sites are not present, showing that the steps behavior is not basically related to the Mn doping. In fact, the same effect has been shown in other compositions such as $La_{0.225}Pr_{0.40}Ca_{0.375}MnO_3$[32] and $(La_{0.3}Eu_{0.2})(Ca_{0.3}Sr_{0.2})$-$MnO_3$.[33] It is worth mentioning that, in all cases, the A site of the perovskite sublattice is partially occupied by magnetic cations. However, we have found that this effect also appears in $La_4Mn_4O_{11}$, where the A position is only occupied by one cation, which is nonmagnetic, whereas the Mn site is not substituted.

On the other hand, most of staircase effect reported in manganites presents steps in the initial magnetization curve. In $La_4Mn_4O_{11}$, the staircase appears not only at the initial magnetization curve but also in the second and fourth quadrants of the hysteresis loop. These differences in the magnetic behavior could be associated with the different magnetic structure adopted by the material as a function of both temperature and applied field.

The relationship between the magnetic behavior and its structure can be explained starting from a magnetic structure close to that shown by layered manganites of the Ruddlesden and Popper series[34] where the FM octahedral layers are AFM

(28) Boulahya, K.; Parras, M.; González-Calbet, J. M.; Amador, U.; Martínez, J. L.; Tissen, V.; Fernández-Díaz, M. T. *Phys. Rev. B* **2005**, *71*, 144402.
(29) Hébert, S.; Hardy, V.; Mahendiran, R.; Hervieu, M.; Martin, C.; Raveau, B. *J. Solid State Chem.* **2002**, *165*, 6.
(30) Hébert, S.; Maignan, A.; Hardy, V.; Martin, C.; Hervieu, M.; Raveau, B. *Solid State Commun.* **2002**, *122*, 335.
(31) Hardy, V.; Hébert, S.; Maignan, A.; Martin, C.; Hervieu, M.; Raveau, B. *J. Magn. Magn. Mater.* **2003**, *264*, 183.
(32) Ghivelder, L.; Freitas, R. S.; das Virgens, M. G.; Continentino, M. A.; Martinho, H.; Granja, L.; Quintero, M.; Leyva, G.; Levy, P.; Parisi, F. *Phys. Rev. B* **2004**, *69*, 214414.
(33) Rana, D. S.; Kuberkar, D. G.; Stone, M. B.; Schiffer, P.; Malik, S. K. *J. Phys.: Condens. Matter* **2005**, *17*, 989.

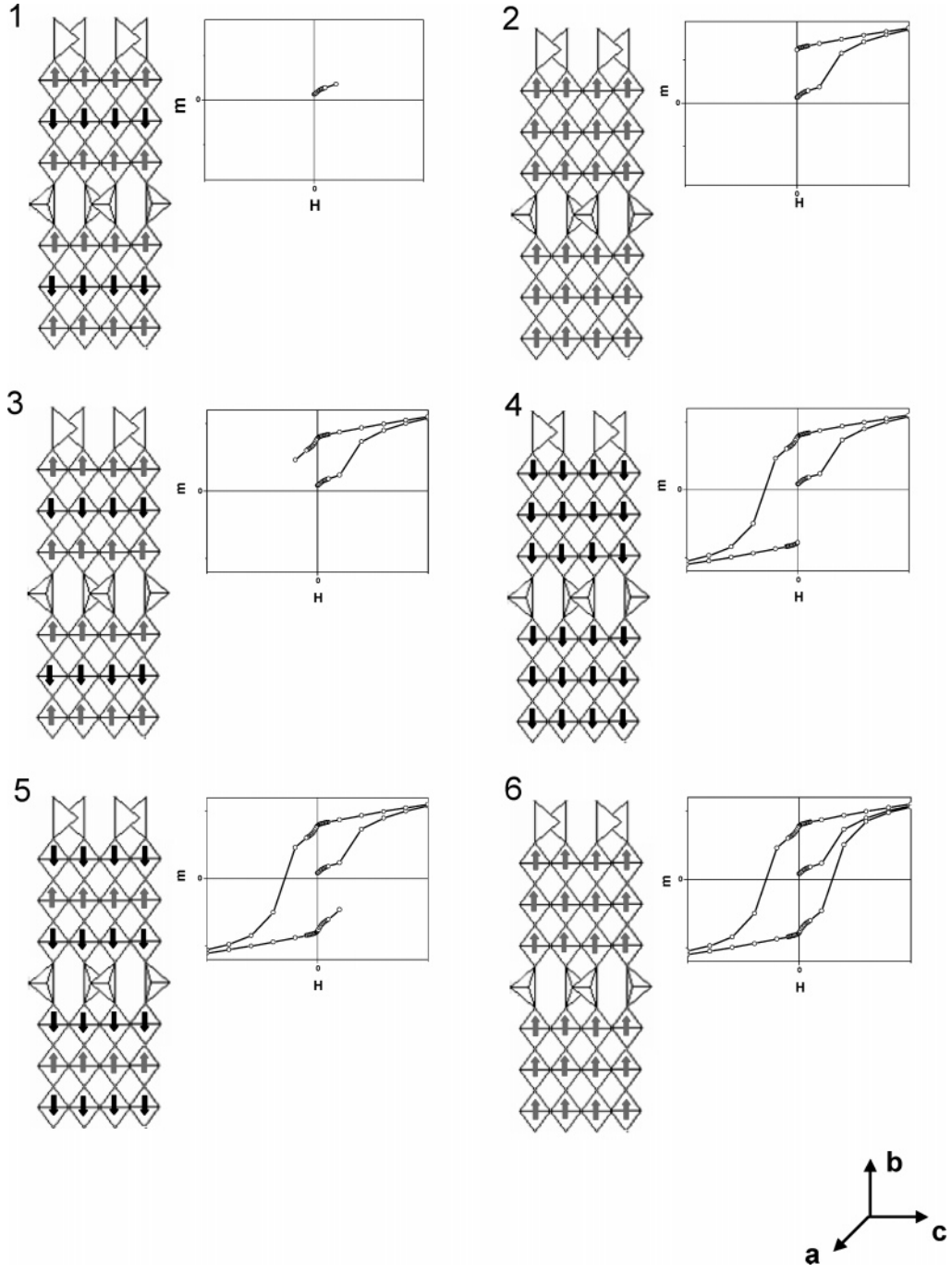

Figure 11. Proposed model showing the evolution of the magnetic behavior as a function of the applied.

coupled in an A-type configuration. In our case, to obtain $La_4Mn_4O_{11}$ we have started from $LaMnO_3$, an A type AFM structure, where Mn atoms are FM coupled within layers parallel to the *ac* plane, these layers being AFM coupled along [010].[4] Taking into account that $La_4Mn_4O_{11}$ is obtained through a topotactic reduction process, it can be assumed that the octahedral layers keep the same A-type AFM structure as the starting material. This ordering only can be observed at the lowest temperatures and until a magnetic field value lower than H_c. Once $H > H_c$, the material shows a FM behavior.

In fact, the linear behavior of the inverse of the magnetization is modified for $H \leq H_c$ at $T \sim 130$ K (see Figure 8). This temperature corresponds to the establishment of an A-type AFM ordering at the octahedral layers as happens in $LaMnO_3$. The same features are observed in the Figure 10a. The formation of steps around 0.2 T can be understood as a consequence of the appearance of different magnetic behavior as a function of magnetic field, and as a consequence, a staircase shape in the hysteresis loop takes place. According to these results, it can be assumed that $La_4Mn_4O_{11}$ shows a magnetic transition (noncompensated AFM to FM) at low temperature induced by the magnetic applied field, that is, a metamagnetic transition.[29−33]

(34) Ling, C. D; Millburn, J. E.; Mitchell, J. F.; Argyriou, D. N.; Linton, J.; Bordallo, H. N. *Phys. Rev. B* **2000**, *62*, 15096.

In agreement with these experimental data, the staircase effect observed at the initial magnetization curve of $La_4Mn_4O_{11}$ seems to be due to the fact that the A-type AFM ordering in the three octahedral layers of the eightfold superstructure is not compensated (Figure 11, stage 1). This situation is kept in a narrow range, and once a critical magnetic field is reached, an inversion of the Mn magnetic moments takes place (Figure 11, stage 2). At this point, all spins are aligned in the applied field direction and an increase of the magnetization value appears. FM ordering remains until zero applied field, where a noncompensated A-type AFM ordering appears again (Figure 11, stage 3), which is kept down to −0.2 T. Once this critical field is reached, an inversion of the magnetic moments, aligned along the field direction, takes place leading to FM behavior (Figure 11, stage 4). The noncompensated AFM ordering is again recovered to zero applied field through the same range of the initial magnetization curve (Figure 10, stage 5). Finally, all spins are again aligned along the field direction (Figure 10, stage 6) to end the loop.

This model accounts for the magnetic behavior from a qualitative point of view. However, from a quantitative one, remnant and saturation magnetization values would not be in agreement with the experimental ones (Table 2). These discrepancies could be related to a possible spin canting of the octahedral layers, as observed in FM $Ba_5Co_5O_{14}$, which shows a saturation magnetization value of 1.3 μ_B in spite of the higher values of Co(IV) (5.9μ_B) and Co(III) (5.4μ_B) magnetic moments.[28]

Conclusions

The ensemble of these results allow the conclusion that the $n = 4$ term of the homologous series $A_nB_nO_{3n-1}$ has been stabilized in the La−Mn−O system according to the $La_4Mn_4O_{11}$ composition, where three [MnO_6] octahedral layers and one [MnO_4] tetrahedral layer intergrow in an ordered way along *b*. Taking into account the oxygen content, this phase must involve manganese in two oxidation states, Mn^{2+} and Mn^{3+}. Taking into account that Mn^{2+} shows preference for tetrahedral coordination in oxygen deficient perovskites,[16] it can be assumed that in $La_4Mn_4O_{11}$, Mn^{2+} occupies the tetrahedral sites and one-third of the octahedral ones, the remaining octahedra being occupied by Mn^{3+} ions. This material presents a FM behavior with $T_c \approx 50$ K, and a staircase effect in the hysteresis loops appears at lower temperatures. This phenomenon seems to be associated to the A-type AFM ordering in the octahedral layers which is kept in the topotactic reduction $LaMnO_3 \rightarrow LaMnO_{2.75}$. Hence, $La_4Mn_4O_{11}$ shows a magnetic field induced transition (noncompensated AFM to FM), that is, a metamagnetic transition, and as a consequence of this metastable state, a staircase effect in the hysteresis loop appears.

Acknowledgment. Financial support trough research Project No. MAT2004-01248 is acknowledged.

CM0609193